Adiabatic chaos in Josephson-junction arrays

A. A. Chernikov and G. Schmidt
Stevens Institute of Technology, Hoboken, New Jersey 07030
(Received 20 June 1994)

Josephson junction arrays made up of units with slightly different parameters are studied. When four or more such units are coupled, the system exhibits global adiabatic Hamiltonian chaos. The case of four units is studied in detail numerically as well as analytically.

PACS number(s): 05.45.+b

I. INTRODUCTION

Arrays of coupled Josephson junctions are an important and interesting example of globally coupled nonlinear oscillators, and have recently received much attention. In particular, Watanabe and Strogatz have recently proved that N identical weakly coupled Josephson-junction oscillators when averaged over fast variables form a completely integrable system.

Here we study the case when the individual junctions are not completely identical. Surprisingly one finds that if $N \geq 4$ the deviation of the parameters of only one unit from those of the others leads to the complete breakdown of integrability and large scale chaotic behavior even for the weakly coupled and averaged systems. For this case one can cast the equations describing the system in a Hamiltonian form.

Due to the Hamiltonian formulation of the problem, it is of interest beyond the special case of weakly coupled Josephson junctions. The best known case of the breakdown of integrability in Hamiltonian systems is related to the Kolmogorov-Arnold-Moser (KAM) theorem [1]. This describes the motion governed by the Hamiltonian $H=H_0+\varepsilon H_1$, where the unperturbed Hamiltonian H_0 is integrable and nondegenerate $|\partial^2 H_0/\partial I_i \partial I_j| \neq 0$. It is well known that the trajectories of motion governed by H_0 are situated on tori with irrational as well as rational winding numbers. As the nonintegrable small εH_1 term is introduced, the rational tori create island chains and chaotic separatrices, while most irrational tori survive. As ε is increased, chaos spreads gradually, with the destruction of more invariant tori and destabilization of stable periodic orbits, the generators of island chains.

One of the first degenerate systems studied was the stochastic web [2], where the two dimensional surface of a section contains circles describing integrable motion, embedded in a thin chaotic stochastic web, whose width increases with increasing ε. The motion on the web is similar to Arnold diffusion in higher dimensional nondegenerate systems.

A more recent example comes from fluid flow in convective cells [3]. Here H_0 gives rise to flow along topological circles rather than tori. For small ε most circles turn into tori, and stable and unstable periodic orbits arise. Again the loss of integrability is gradual with increasing ε.

Weakly coupled Josephson junctions in the limit treated here are another case of a degenerate Hamiltonian system, with properties very different from the previous examples. There are two integrable limits. In the first, when all junctions are identical, the trajectories are topological circles embedded in tori. To illustrate the second case, let us take $N=4$, which is the smallest N to permit transition to nonintegrability. If two pairs are identical (say $r_1=r_3$ and $r_2=r_4, r_1 \neq r_2$) the system is integrable. Two types of trajectories on a torus are now possible: topological circles and closed curves that cannot be transformed to circles on the torus.

Nonintegrability arises when, e.g., $r_1=r_2=r_3$, $r_4=r_1+\varepsilon$, or $r_1=r_2, r_3=r_4+\varepsilon$. The motion becomes chaotic in a large volume of the phase space, no matter how small ε is, in marked contrast to the nondegenerate case.

For $N=4$ some limits are amenable to analytical treatment. When the integrable case contains the two types of closed curves on the torus, a separatrix divides the regions of the torus which contain these curves. In the weakly nonintegrable case adiabatic invariants can be associated with the circles as well as the curves outside the separatrix. As the system evolves, separatrix crossing result in chaotic changes in the adiabatic invariants, and adiabatic chaos arises.

The paper is organized as follows. Section II presents basic equations on Josephson-junction arrays, and briefly reviews most relevant previous results. In Sec. II B we consider an averaged system of nonidentical globally coupled oscillators.

In Sec. III we give a description of the dynamics. Section III A gives a qualitative picture of the dynamics in multidimensional space based on computer simulations. Section III B describes qualitatively a dynamics of four coupled oscillators. In Sec. III C the process of trapping into resonance is considered.

II. BASIC EQUATIONS

A. Equations for resistively loaded one-dimensional Josephson-junction arrays

We will restrict ourselves to the simplest and most frequently studied case, in which N point-contact Josephson

junctions with different resistance r_i are connected in series [4–6]. We will assume that bias current I_b is constant and is shunted by pure resistive load R (Fig. 1). From Kirchhoff's current and voltage laws it follows that

$$(\hbar/2er_i)d\varphi_i/dt+I_{ci}\sin\varphi_i+I=I_b\ ,$$
$$RI=(\hbar/2e)\sum_{i=1}^{N}d\varphi_i/dt\ . \tag{2.1}$$

Here $\hbar=h/2\pi$, and h is Planck's constant, e is the electron charge, φ_i is a phase difference across the individual junction, I_{ci} is the junction's critical current, and I is the current flowing through resistor R. The Josephson relations for supercurrent I_i and voltage V_i are supposed to be valid for individual junction i:

$$I_i=I_{ci}\sin\varphi_i,\quad V_i=(\hbar/2e)d\varphi_i/dt\ .$$

From (2.1) it follows that

$$(\hbar/2er_i)d\varphi_i/dt+I_{ci}\sin\varphi_i+(\hbar/2eR)\sum_{j=1}^{N}d\varphi_j/dt=I_b\ . \tag{2.2}$$

Multiplying (2.2) by r_i leads, after summation, to

$$(\hbar/2e)\sum_{i=1}^{N}d\varphi_i/dt=\left[NI+\sum_{i=1}^{N}r_iI_{ci}\sin\varphi_i\right]R_0/(R_0+r_0)\ , \tag{2.3}$$

where

$$R_0=R/N,\quad r_0=(1/N)\sum_{i=1}^{N}r_i\ ,$$

Substituting (2.3) into (2.2) gives

$$(\hbar/2er_i)(R_0+r_0)d\varphi_i/dt=I_bR_0-I_{ci}(R_0+r_0)\sin\varphi_i+(1/N)\textstyle\sum r_iI_{ci}\sin\varphi_i\ . \tag{2.4}$$

We want to study cases where the resistances r_i as well as the Josephson junctions characterized by I_{ci} are nearly identical. So one introduces the averaged critical current

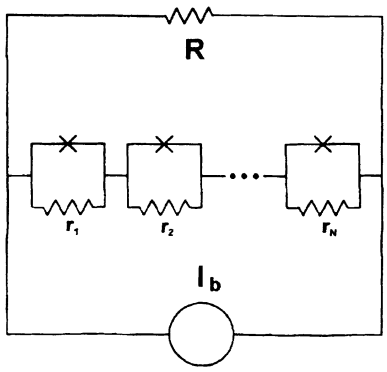

FIG. 1. A resistively shunted series array of Josephson junctions.

$$I_{e0}=(1/N)\sum_{i=1}^{N}I_{ci}\ ,$$

as well as the normalized deviations from the averages:

$$\zeta_i=(r_i-r_0)/r_0\ \text{ and }\ \chi_i=(r_iI_{ci}-r_0I_{c0})/r_0I_{c0}\ ,$$

to obtain from (2.4), after dividing by I_bR_0,

$$(\hbar/2e)(R_0^{-1}+r_0^{-1})I_b^{-1}(1+\zeta_i)^{-1}d\varphi_i/dt=1-(R_0^{-1}+r_0^{-1})I_b^{-1}r_0I_{c0}(1+\chi_i)(1+\zeta_i)^{-1}\sin\varphi_i+(r_0I_{c0}/NI_bR_0)\sum_{j=i}^{N}(1+\chi_j)\sin\varphi_j\ . \tag{2.5}$$

Now we introduce a rescaled time

$$(\hbar/2e)(R_0^{-1}+r_0^{-1})I_b^{-1}d/dt\rightarrow d/dt$$

and

$$a=-I_{c0}r_0(R_0^{-1}+r_0^{-1})/I_b,\quad \varepsilon=I_{c0}r_0/NI_bR_0$$

to obtain

$$d\varphi_i/dt=1+\zeta_i+a(1+\chi_i)\sin\varphi_j+\varepsilon(1+\zeta_i)\sum_{j=1}^{N}(1+\chi_j)\sin\varphi_j\ . \tag{2.6}$$

It is convenient to shift the phase $\varphi_i=\eta_i+\pi/2$, to obtain the equation

$$d\eta_i/dt=1+\zeta_i+a(1+\chi_i)\cos\eta_i+\varepsilon(1+\zeta_i)\sum_{j=1}^{N}(1+\chi_j)\cos\eta_j\ .$$

If ε is small (say N, or R_0/r_0 is large), and so are deviations from the average, and second order small terms are ignored, this equation reduces to

$$d\eta_i/dt=1+\zeta_i+a(1+\chi_i)\cos\eta_i+\varepsilon\sum_{j=1}^{N}\cos\eta_j\ . \tag{2.7}$$

Two symmetries of this system should be noted. The equations are invariant under permutation of the N indices (if $\zeta_i=\chi_i=0$), and under simultaneous time and coordinate reversal $t\rightarrow -t$ and $\eta_i\rightarrow-\eta_i$. The latter means that the equation belongs to the class of reversible systems [7] which possesses properties of both Hamiltonian and dissipative systems.

B. Averaged system

Progress in studying Eq. (2.7) for $N>2$ can be achieved by introducing some separation of time scales and averaging over fast motion. As a ground state it is reasonable to consider the limit of uncoupled identical oscillators. Then the averaging procedure can be performed as follows [5]. Let us first change variables

$$(d\eta_i/dt)/(1+a\cos\eta_i)=C(d\vartheta_i/dt)\ , \tag{2.8}$$

where

$$C=(1/2\pi)\int_0^{2\pi} d\eta/(1+a\cos\eta)=[1-a^2]^{-1/2}$$

is the normalization multiplier. By integrating (2.8), one can connect new variables ϑ_i with η_i:

$$\tan\vartheta_i/2=\{(1-a)/(1+a)\}^{1/2}\tan\eta_i/2 \ . \tag{2.9}$$

Instead of (2.7), we obtain

$$\dot\vartheta_i=1+[(\zeta_i+z\chi_i)\cos\eta(\vartheta_i)]/[1+a\cos\eta(\vartheta_i)] +\varepsilon\sum_{j=1}^{N}\cos\eta(\vartheta_j)/(1+\mathbf{a}\cos\eta(\vartheta_i)) \ . \tag{2.10}$$

We will seek a solution of (2.10) in the form $\vartheta_i=t+\theta_i$, where $\dot\theta_i\sim\varepsilon$, i.e., variables θ_i are slow. Averaging (2.10) over the fast period, we obtain

$$\dot\theta_i=(1/2\pi)\int_0^{2\pi}[(\zeta_i+a\chi_i)\cos\eta(t)]/[1+a\cos\eta(t)]dt+\varepsilon\sum_{j=1}^{N}(1/2\pi)\int_0^{2\pi}\cos\eta(t)/[1+a\cos\eta(t+\theta_i-\theta_j)]dt \ . \tag{2.11}$$

The integrals on the right-hand side of (2.11) can be evaluated exactly using the following relation:

$$1+a\cos\eta(\psi)=(1-a^2)/(1-a\cos\psi) \ ,$$

which is a direct consequence of (2.9). After integration, we obtain

$$\dot\theta_i=(\zeta_i-a\chi_i)/(1-a^2)+\varepsilon N[(1-a^2)^{1/2}-1]/a(1-a^2)+(\varepsilon/a)[1-(1-a^2)^{-1/2}]\sum_{j=1}^{N}\cos(\theta_i-\theta_j) \ . \tag{2.12}$$

The second term on the right-hand side of (2.12) can be removed by a simple phase shift. After evident rescaling of time, we finally obtain

$$\dot\theta_i=\omega_i+\sum_{j=1}^{N}\cos(\theta_i-\theta_j) \tag{2.13}$$

This equation is an obvious generalization of the averaged equation, derived in Ref. [5] for identical oscillators,

$$\omega_i=(a/\varepsilon)(\zeta_i-a\chi_i)/[1-a^2-(1-a^2)^{1/2}] \ .$$

III. MULTIDIMENSIONAL CHAOS

A. Qualitative analysis of computer simulations

In this section we give a preliminary qualitative analysis which demonstrates how the dynamics of the averaged system (2.13) depends on the dimension of phase space (or on the numbers N of nonlinear oscillators). If $N\le 3$, the system is integrable. If only three oscillators are coupled, from Eq. (2.13) it follows that

$$\begin{aligned}\dot\xi_1&=\delta_1+\cos(\xi_1+\xi_2)-\cos(\xi_2) \ ,\\ \dot\xi_2&=\delta_2-\cos(\xi_1+\xi_2)+\cos(\xi_1) \ ,\end{aligned} \tag{3.1}$$

where

$$\xi_1=\theta_1-\theta_2, \quad \xi_2=\theta_2-\theta_3 \ ,$$

$$\delta_1=\omega_1-\omega_2, \quad \delta_2=\omega_2-\omega_3 \ .$$

System (3.1) is one degree of the freedom Hamiltonian system

$$\dot\xi_1=\partial H/\partial\xi_2, \quad \dot\xi_2=-\partial H/\partial\xi_1 \ , \tag{3.2}$$

with the Hamiltonian

$$H(\xi_1,\xi_2)=\delta_1\xi_2-\delta_2\xi_1-\sin\xi_1-\sin\xi_2+\sin(\xi_1+\xi_2) \ . \tag{3.3}$$

Two phase portraits of Eq. (3.2) [contours $H(\xi_1,\xi_2)=\text{const}$] are shown in Figs. 2(a) and 2(b). They are both periodic in the (ξ_1,ξ_2) plane with 2π periodicity. Figure 2(a) for $\delta_1=\delta_2=0$ contains only regions of finite dynamics, while in Fig. 2(a) for $\delta_1=0.2$ and $\delta_2=0.2$ the structural degeneracy is removed and the phase portrait contains both regions of finite and infinite periodic motions.

If $N=4$ then the system (2.13) is no longer integrable. Figure 3(a) illustrates the projection of the typical trajectory on the (θ_1,θ_2) plane. The trajectory consists of springlike pieces with different diameters and their axes directed at three different angles in the phase space $(\theta_1,\theta_2,\theta_3)$. The lengths of all springs are approximately the same, but the diameters differ significantly. The trajectory performs random walks between these springs. Such walks are superimposed with ballistic motion averaged over the phase space velocity $\dot{\boldsymbol\xi}=\boldsymbol\omega$. At the intersection between different spirals several interesting phenomena take place. First of all, the trajectory may either continue its motion in the same direction or make a turn. This choice looks random, and depends sensitively on initial conditions. Then sharp changes in the spirals diameters take place at the intersections which appear random as well. Finally the direction of rotation changes its sign at the intersection. This motion strongly resembles the motion of a charged particle in a magnetic field with abrupt changes of direction. The helical motion corresponds to the cyclotron rotation, and motion along the spring axes corresponds to the drift of a guiding center. As is well known, the most powerful tool for the study of such dynamics is drift equations which presume the conservation of certain adiabatic invariants. In our model

the spiraling motion is fast, with characteristic frequency $\Omega_{sp}\sim 1$, while the motion of the "guiding center" is slow with characteristic frequency $\Omega_{guide}\sim\omega$. Thus averaged over fast frequency, motion should conserve certain adiabatic invariants. On the other hand, as we mentioned above, the direction of rotation changes its sign between two different springs. It means that somewhere the frequency $\Omega_{sp}=0$, and the adiabatic invariant is no longer conserved. As we shall see below, the sharp change in the helix diameters, corresponds to the adiabatic invariant jump between two different regimes of motion.

Our computer simulations suggest that basic characteristic features of the nonlinear dynamics do not qualitatively change if the number of coupled oscillators grows. For example, Fig. 3(b) represents the projection of the trajectory on the θ_1,θ_2 plane for $N=5$. One can see a definite similarity in both pictures—the trajectories in phase space consist of springlike pieces. The number of different directions of axes of such spirals in phase space grow with N, and the transition between different spirals is smoother in higher dimensional space.

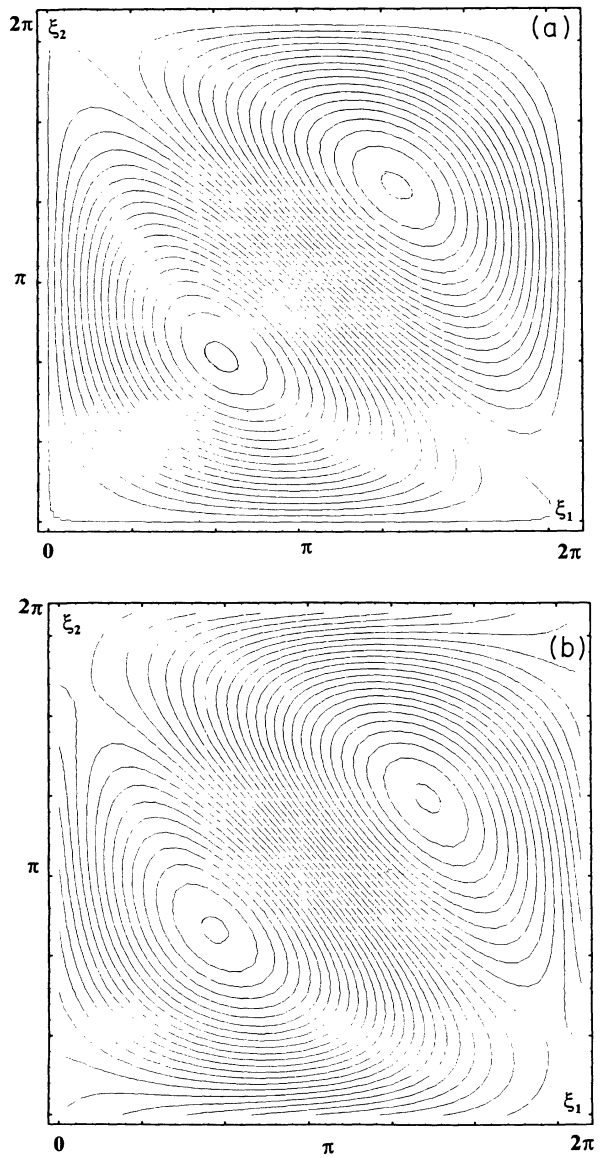

FIG. 2. The contour levels of the Hamiltonian (3.3). (a) $\delta_1=\delta_2=0$. (b) $\delta_1=\delta_2=0.2$.

B. Nonintegrable dynamics of four oscillators

Equations (2.13) for four coupled oscillators

$$\begin{aligned}
\dot\theta_1&=\omega_1+1+\cos(\theta_1-\theta_2)+\cos(\theta_1-\theta_3)+\cos(\theta_1-\theta_4)\ ,\\
\dot\theta_2&=\omega_2+\cos(\theta_2-\theta_1)+1+\cos(\theta_2-\theta_3)+\cos(\theta_2-\theta_4)\ ,\\
\dot\theta_3&=\omega_3+\cos(\theta_3-\theta_1)+\cos(\theta_3-\theta_2)+1+\cos(\theta_3-\theta_4)\ ,\\
\dot\theta_4&=\omega_4+\cos(\theta_4-\theta_1)+\cos(\theta_4-\theta_2)+\cos(\theta_4-\theta_3)+1
\end{aligned}\tag{3.4}$$

in new variables

$$\begin{aligned}
x_1&=(\theta_1-\theta_2+\theta_3-\theta_4)/2\ ,\\
x_2&=(\theta_1-\theta_3+\theta_2-\theta_4)/2\ ,\\
x_3&=(\theta_1-\theta_2+\theta_4-\theta_3)/2
\end{aligned}$$

can be transformed to a more convenient form:

$$\begin{aligned}
\dot x_1&=\varepsilon_1+\sin(x_2)\sin(x_3)\ ,\\
\dot x_2&=\varepsilon_2+\sin(x_1)\sin(x_3)\ ,\\
\dot x_3&=\varepsilon_3+\sin(x_1)\sin(x_2)\ .
\end{aligned}\tag{3.5}$$

Here the frequency mismatches are

$$\begin{aligned}
\varepsilon_1&=(\omega_2-\omega_1+\omega_4-\omega_3)/4\ ,\\
\varepsilon_2&=(\omega_4-\omega_1+\omega_3-\omega_2)/4\ ,\\
\varepsilon_3&=(\omega_2-\omega_1+\omega_3-\omega_4)/4\ ,
\end{aligned}$$

and time has been rescaled ($t'=-2t$).

Two important conclusions follow immediately from (3.5).

(1) Flow in the x_i space is incompressible $\sum_{(i)}\partial\dot x_i/\partial x_i=0$, and it can be cast in a Hamiltonian form (see the Appendix).

(2) Defining the vectors $\dot{\mathbf{x}}$ and $\boldsymbol{\varepsilon}$, it is clear that the flow velocity when averaged over $\mathbf{x}$ space is $\langle\dot{\mathbf{x}}\rangle=\boldsymbol{\varepsilon}$.

Now we study that if only one of the ε_i's is nonzero, the system is integrable. Take, e.g., $\varepsilon_3\neq 0$ and $\varepsilon_1=\varepsilon_2=0$. Divide the first two equations of (3.5) to obtain $\sin(x_1)dx_1=\sin(x_2)dx_2$, or

$$\cos x_1-\cos x_2=C_1\ .\tag{3.6}$$

Dividing the third equation by the first gives

$$\begin{aligned}
dx_3/dx_1&=[\varepsilon_3/\sin x_2+\sin x_1]/\sin x_3\\
&=[\varepsilon_3/\sqrt{1-(C_1-\cos x_1)^2}+\sin x_1]/\sin x_3\ ,
\end{aligned}$$

resulting in

$$\cos(x_1)-\cos(x_3)-\varepsilon_3\int dx_1/\sqrt{1-(C_1-\cos x_1)^2}=C_2 \ . \tag{3.7}$$

Equation (3.6) defines cylinders parallel with the x_3 axis (see Fig. 4). In the vicinity of the $x_1=0$, $x_2=\pi$ (or $x_1=\pi$, $x_2=0$) axes, one may expand $\delta x_1=x_1$, $\delta x_2=x_2-\pi$ to obtain, from (3.6),

$$\delta x_1^2+\delta x_2^2\equiv\rho_0^2=\text{const} \ , \tag{3.8}$$

or introducing cylindrical variables (ρ,θ,z), where the z axis coincides with the axis of the spring $\delta x_1=\rho\cos\theta$, $\delta x_2=\rho\sin\theta$, and $x_3=z$, from (3.5) it follows that

$$\dot{\theta}=\sin(z) \tag{3.9}$$

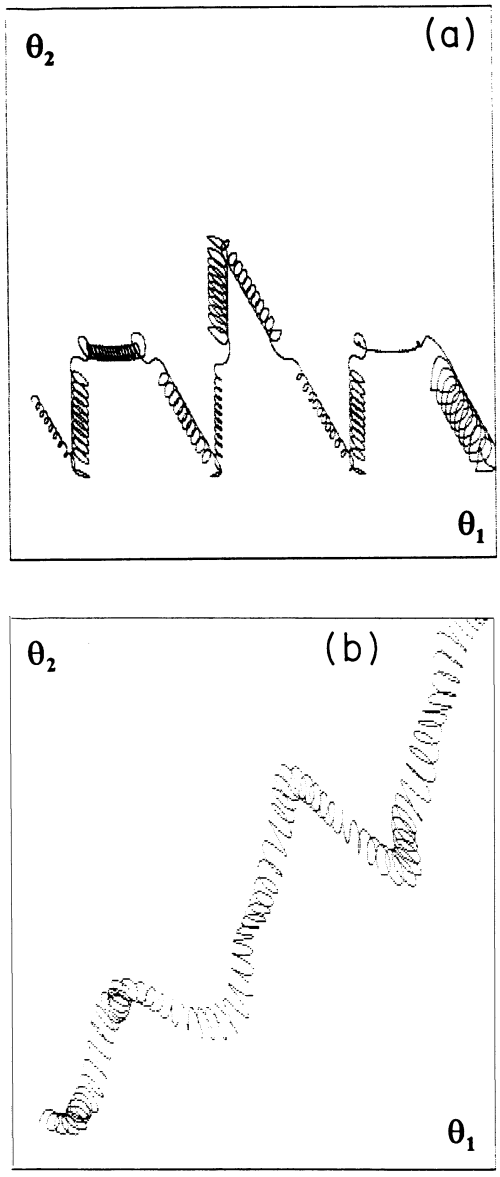

FIG. 3. The projection of the typical trajectory of system (2.13) on (θ_1,θ_2) plane. (a) $N=4$. (b) $N=5$.

and

$$\dot{z}=\varepsilon_3-(\rho_0^2/2)\sin2\theta \ . \tag{3.10}$$

Equations (3.9) and (3.10) correspond to the Hamiltonian system with one degree of freedom:

$$\dot{\theta}=-\partial H/\partial z, \quad \dot{z}=\partial H/\partial\theta \ , \tag{3.11}$$

where the Hamiltonian

$$H(z,\theta)=(\rho_0^2/4)\cos2\theta+\varepsilon_3\theta+\cos(z) \tag{3.12}$$

is the second constant of motion. Equations $\rho=\text{const}$ and $H(z,\theta)=\text{const}$ determine the helical trajectory in phase space ρ,θ,z (see Fig. 5). The phase portrait of systems (3.11) and (3.12) depends on two parameters, the radius of helix ρ_0, and the frequency mismatch ε_3. Figures 6(a) and 6(b) illustrate phase portraits of (3.10) for two different values of radius ρ_0 and a fixed value of $\varepsilon_3=0.4$. There are two different types of phase portraits; the first type [Fig. 6(a)] $\rho_0^2<2\varepsilon_3$ contains only periodic trajectories that correspond to rotation and no stagnation points are present, while the phase portraits of the second type $\rho_0^2>2\varepsilon_3$ contain both rotating and oscillating trajectories [Fig. 6(b)], and a saddle point as well as a separatrix appears. Stagnation points on Figs. 6(b) with coordinates (z_a,θ_a)

$$\sin z_a=0, \quad 2\varepsilon_3=\rho_0^2\sin2\theta_a \tag{3.13}$$

exist if the radius of a helix is not too small $(\rho_0^2\geq2\varepsilon_3)$. At $\rho_0=\rho_{\text{bif}}=(2\varepsilon_3)^{1/2}$ there is a bifurcation in the phase portrait, and simultaneous birth of elliptic and hyperbolic stagnation points.

Of course, the same situation arises when $\varepsilon_1\neq0$, $\varepsilon_2=\varepsilon_3=0$, etc. Figure 7 shows the cylinder axes. When more than one $\varepsilon_i\neq0$, the motion is no longer integrable, but for ε_i sufficiently small a qualitative interpretation

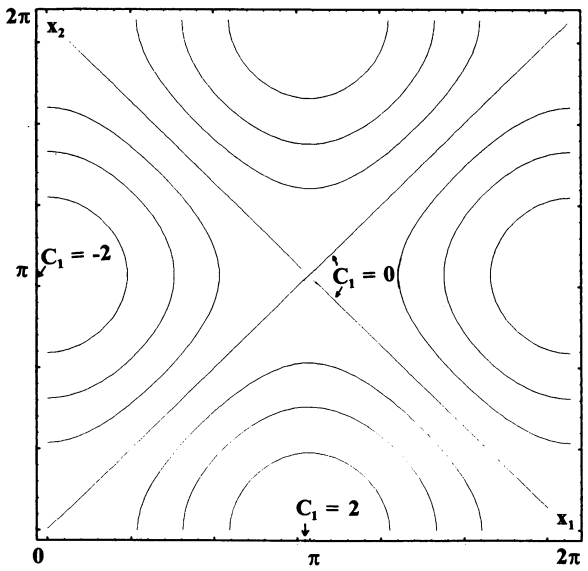

FIG. 4. The contour levels of the first integral (3.6).

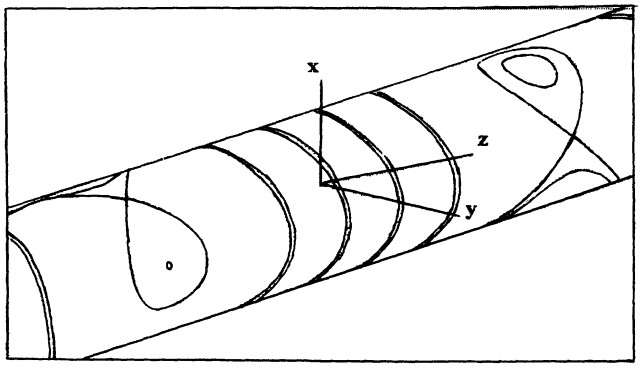

FIG. 5. The helical and circular trajectories in phase space.

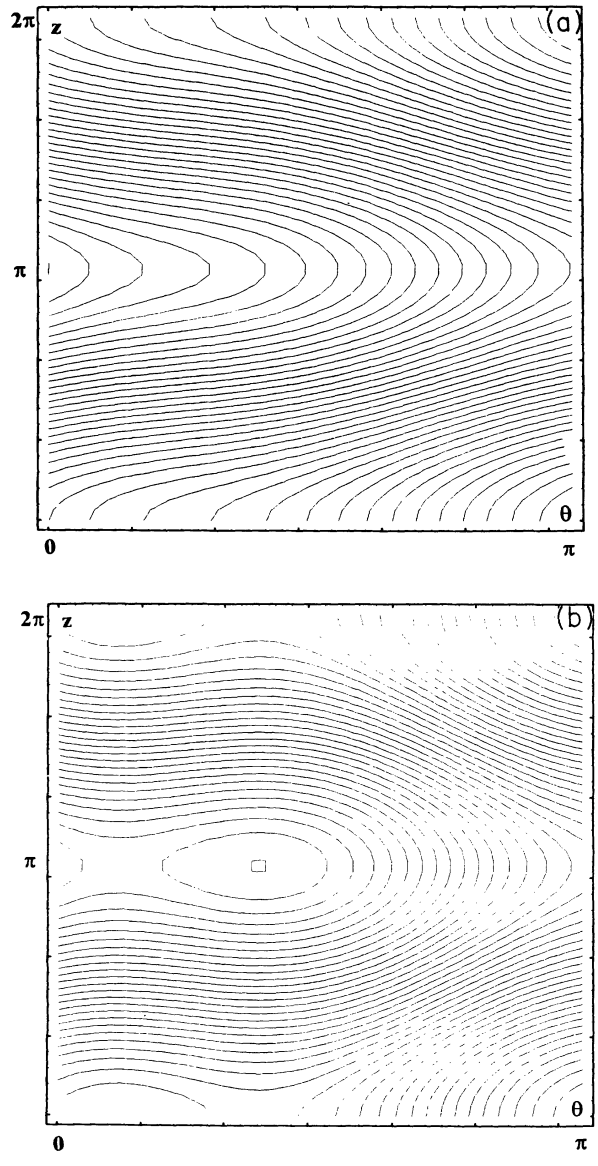

FIG. 6. The contour levels of the Hamiltonian (3.12). (a) $\varepsilon_3=0.4, \rho_0^2=0.4$. (b) $\varepsilon_3=0.4, \rho_0^2=1.2$.

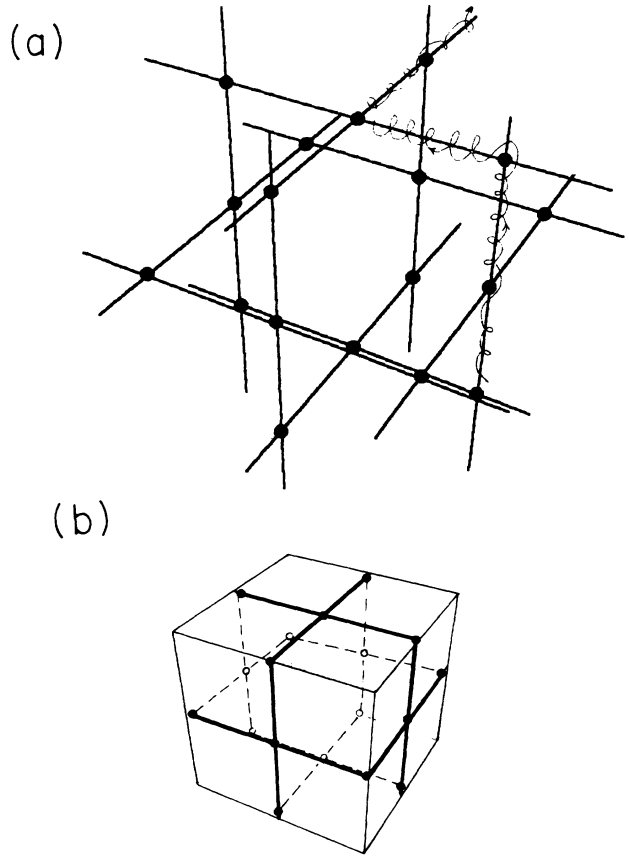

FIG. 7. The network in the phase space of system (3.5). (a) A trajectory performs random walks between black dots. (b) Geometrical arrangement of the cylinder axes. Black dots indicate their intersection points.

can be given to the computational results shown in Fig. 3(a). The springlike trajectories correspond to motion on a cylinder between the intersection points of Fig. 7, while near an intersection point the trajectory may switch to a cylinder with an axis perpendicular to that of the first cylinder. Note also that the closed orbits of the integrable case in Fig. 6(a) appear at $z=\pi n$ (n is an integer), where the axes intersect. When all three $\varepsilon_i \neq 0$, the same expansion near the axis ($\rho \ll 1$) leads to

$$\begin{aligned} \dot{\rho} &= \varepsilon_1 \cos\theta + \varepsilon_2 \sin\theta \ , \\ \rho\dot{\theta} &= \rho \sin(z) - \varepsilon_1 \sin\theta + \varepsilon_2 \cos\theta \ , \\ \dot{z} &= \varepsilon_3 - (\rho^2/2)\sin 2\theta \ . \end{aligned} \tag{3.14}$$

If ε_1 and ε_2 are nonzero, then the radius of the spiral slowly changes in time according to Eq. (3.14), and there exists a switching between different cylinders. As a result initially open trajectories in Fig. 5 can cross the separatrix and become trapped or vice versa. This process leads to switching between cylinders. In Sec. III C a quantitative analysis of the switching will be given.

C. Trapping into resonance

In the limiting case when $\varepsilon_i \to 0$, one can analytically estimate the probability of switching. Let us modify the Hamiltonian (3.12)

$$h(\rho,z,\theta) = -1+\cos(z)+(\rho^2/4)\{\cos 2\theta - \cos 2\theta_a\} + \varepsilon_3(\theta-\theta_a) \tag{3.15}$$

in such a way that it is equal to zero ($h=0$) at the separatrix passing through the saddle point with coordinates $z=0$ and $\theta=\theta_a$. If $\varepsilon_1 \neq 0$ or $\varepsilon_2 \neq 0$, then parameter $\rho^2(t)$ in (3.15) slowly evolves in time according to (3.14). The separatrix of (3.15) with fixed parameter ρ,

$$z_s(\rho,\theta) = \arccos\{1-(\rho^2/4)[\cos 2\theta - \cos 2\theta_a] - \varepsilon_3(\theta-\theta_a)\}\ , \tag{3.16}$$

discriminates two types of motion: rotation around the cylindrical surface and oscillations near an elliptical point (see Fig. 8). It forms a loop with a knot at the saddle point. Let θ_e be the point where the loop crosses the $z=0$ axis. As ρ evolves, an initially oscillating trajectory may become a rotating one. The opposite transition from rotation to oscillation can occur as well. In such a case an initially rotating point will eventually be trapped when its trajectory is overcome by the growing separatrix loop. In Fig. 8 two actual trajectories are shown by dashed lines. They cross line $\theta=\theta_a$ in points b and d. The rotating trajectories that cross that line between points a and b will cross the separatrix and become trapped. The trajectory that crosses the line between points b and d will remain in a rotating regime until the next passage through resonance.

We calculate the probability that a trajectory becomes trapped during one passage through resonance. The trapping probability is calculated [8,9] by taking the ratio of phase volume fluxes that pass between a and b to those that pass between a and d. The flux F of the phase space area crossing a line spanned by points 1 and 2 is

$$F_{1,2} = \left| \int_1^2 d\mathbf{l} \times \dot{\mathbf{q}} \right| = h_2 - h_1\ , \tag{3.17}$$

where $d\mathbf{l}$ is a line element on the phase plane, and $\dot{\mathbf{q}} = (\dot{z},\dot{\theta}) = (\partial h/\partial\theta, -\partial h/\partial z)$ is the phase flow velocity. In evaluating the phase flux we neglect the integration along the third dimension, since ρ changes slowly in time in comparison with z and θ. The trapping probability is then

$$W = \frac{F_{ab}}{F_{ad}} = \frac{h_b}{h_c + (h_d - h_c)}\ . \tag{3.18}$$

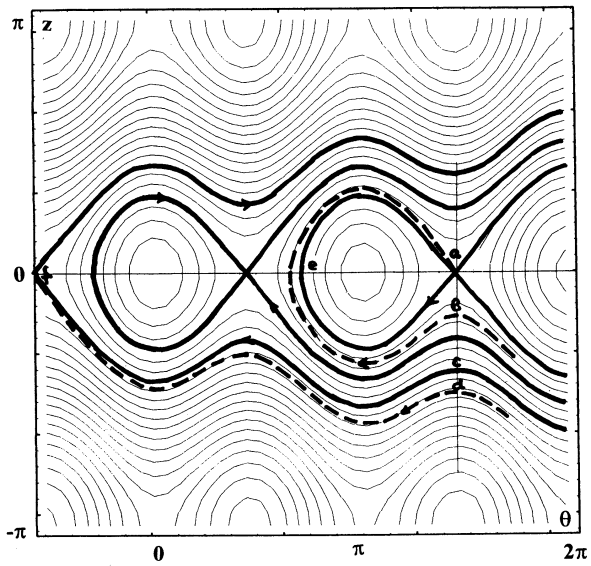

FIG. 8. The phase portrait corresponding to the Hamiltonian (3.15). The thickest lines are the separatrices. Dashed thick lines represent actual trajectories of Eqs. (3.14).

If $\varepsilon_i \to 0$, one can evaluate h_b and $h_d - h_c$ as the integrals [10]

$$h_b \approx -\Theta_1 = -\oint_{\mathcal{L}_1} dt\{\dot{\rho}\partial h/\partial\rho + \dot{\theta}\partial h/\partial\theta + \dot{z}\partial h/\partial z\}\ , \tag{3.19}$$

$$h_d - h_c \approx -\Theta_2 = -\int_{\mathcal{L}_2} dt\{\dot{\rho}\partial h/\partial\rho + \dot{\theta}\partial h/\partial\theta + \dot{z}\partial h/\partial z\}\ ,$$

where contour $\mathcal{L}_1$ is a separatrix loop in Fig. 8, and contour $\mathcal{L}_2$ is the upper branch of the separatrix connecting points c and f. Therefore it is useful to consider the phenomenon of trapping as a random event. Such an approach was first used in Ref. [11]. The general methods of evaluating trapping probability is given by Neishtadt [8]. The probability W of trapping into the loop with the saddle at point a in Fig. 8 is

$$W = \Theta_1/(\Theta_2 - h_c)\ . \tag{3.20}$$

The value Θ_i approximates the change of energy along the connected part of the perturbed trajectory, which is near the unperturbed separatrix $\mathcal{L}_i$ ($i=1,2$). We assume that $\Theta_i > 0$. Since $h_c = h_f$ and $\theta_a - \theta_f = 2\pi$, from (3.15)

$$h_c = -2\pi\varepsilon_3\ . \tag{3.21}$$

Equations (3.14), (3.15), and (3.19) lead to the integral representations for $\Theta_{1,2}$:

$$\Theta_{1,2} = -\int_{\mathcal{L}_{1,2}} dt\{(\rho/2)[\varepsilon_1\cos\theta + \varepsilon_2\sin\theta](\cos 2\theta - \cos 2\theta_a) + (1/\rho)(-\varepsilon_1\sin\theta + \varepsilon_2\cos\theta)[(-\rho^2/2)\sin 2\theta + \varepsilon_3]\}\ . \tag{3.22}$$

Using (3.16) and the unperturbed equation of motion along the separatrix, one can integrate over θ instead of integrating over time t:

$$dt = d\theta/\dot{\theta} = d\theta/\sin z = d\theta/\{1-[1-(\rho^2/4)(\cos 2\theta - \cos 2\theta_a) - \varepsilon_3(\theta-\theta_a)]^2\}^{1/2}\ . \tag{3.23}$$

Let us first estimate Θ_1. To evaluate (3.22) and (3.23) we make several assumptions. First, we assume that $1 \gg \rho \gg \sqrt{\varepsilon_3}$, and neglect small terms proportional to ε_3 in (3.23). The right-hand side of (3.22) under these assumptions is significantly simplified:

$$\Theta_1 = -\sqrt{2}\varepsilon_1 \int_{\theta_a}^{\theta_e} d\theta [\cos\theta - \cos(\theta - 2\theta_a)] / |\cos 2\theta - \cos 2\theta_a|^{1/2} + \sqrt{2}\varepsilon_2 \int_{\theta_a}^{\theta_e} d\theta [\sin\theta - \sin(\theta - 2\theta_a)] / |\cos 2\theta - \cos 2\theta_a|^{1/2} . \tag{3.24}$$

Second, we suppose that $z_a = z_e = 0$, $\theta_e \approx 3\pi/2$, and $\theta_e \approx \pi/2$, i.e., we neglect small corrections proportional to ε_3 in the locations of these points. Integrating (3.24) under these assumptions leads to the following expression for Θ_1:

$$\Theta_1 = 2\pi\varepsilon_1 . \tag{3.25}$$

The integration along the lower branch of the separatrix, connecting points c and f, leads, under the same assumptions, to an analogous estimating for $\Theta_2 \approx \Theta_1$. This formula simply indicates that if $\varepsilon_3 \to 0$ the lower branch of the separatrix loop connecting points a and e coincides with the right half of the separatrix, connecting points c and f. The integration along the remaining upper branch of the loop, connecting e and a, is equivalent to the integration along the left half of the separatrix connecting c and f.

Now we are able qualitatively to explain the basis features of the dynamics of system (3.5). Let the trajectory initially rotate around the x_3 axis. Its "guiding center" moves along this axis, passing near separatrix loops in Fig. 9. During every passage near such a loop it has a finite probability to be captured by the loop and change the direction of its "guiding center" velocity. After the capture the guiding center moves along x_1 or x_2 axes (that correspond to $\theta = 0$ or $\theta = \pi/2$, respectively). From (3.20), (3.21), and (3.25) it follows that the probability for the particle to be captured near $\theta = 0$ and move in the x_1 or x_3 direction is given by the formulas

$$W_{3\to 1} \approx \varepsilon_1/(\varepsilon_1 + \varepsilon_3) , \qquad W_{3\to 3} \approx \varepsilon_3/(\varepsilon_1 + \varepsilon_3) . \tag{3.26}$$

The analogous transition can occur near $\theta = \pi/2$. The probability for the trajectory to be captured and move along the x_2 direction is given by Eq. (3.26), where one should substitute $1 \to 2$. The trajectory moves along the x_2 axis exactly in the same way as it moved along the x_3 axis before capture into resonance. While passing near separatrix loops it can be captured again and change its direction to x_1 or x_3.

The web of intersecting cylinders being periodic, they can also be represented as three mutually intersecting tori, as shown in Fig. 10.

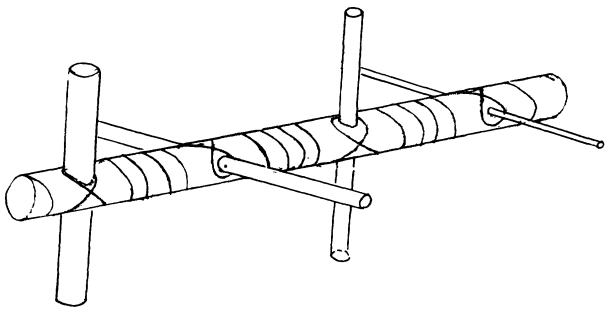

FIG. 9. Passing near the separatrix loops, the trajectory has a finite probability to change its direction and to start to move around the perpendicular cylinder.

IV. SUMMARY

We have studied arrays of Josephson junctions with slightly different parameters. While it is known that arrays of weakly coupled identical junctions lead after averaging to an integrable set of equations [6], we find that integrability breaks down for the more realistic case when the junction parameters differ for $N \geq 4$, where N is the number of connected junctions.

First, simplified averaged equations are derived, and the $N = 3$ case is shown to be integrable. When $N = 4$, while the flow in phase space is incompressible, and can be cast in Hamiltonian form, the system exhibits unusual nonintegrable behavior. In the limit when the parameters ε_i (a measure of differences in junction parameters) are vanishingly small, phase space is characterized by sets of cylinders with axes forming a web of straight lines intersecting perpendicularly (see Figs. 7 and 9).

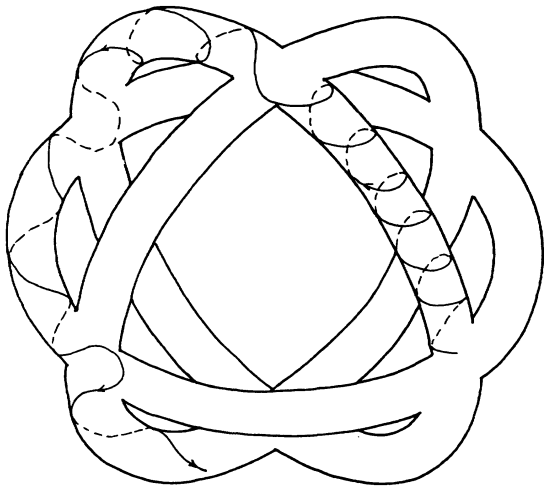

FIG. 10. The mutually intersecting tori represent the network on Fig. 7.

The flow hops from cylinder to (perpendicular) cylinder in an unpredictable chaotic manner. This process is a case of adiabatic chaos, due to separatrix crossings [12]. Analytic expressions for the probability of such a transition are derived. Unlike KAM systems, where a small deviation from integrability results in small chaotic bands among regular trajectories, here an unusual form of global chaos arises where regular and chaotic motions alternate.

APPENDIX: HAMILTONIAN VARIABLES IN THE GENERAL CASE

Let us introduce new notations

$$\begin{aligned}&\xi_1=\theta_1-\theta_2,\quad \xi_2=\theta_2-\theta_3\ ,\\&\xi_3=\theta_3-\theta_4,\quad \xi_4=\theta_4-\theta_1\ ,\\&\delta_1=\omega_1-\omega_2,\quad \delta_2=\omega_2-\omega_3\ ,\\&\delta_3=\omega_3-\omega_4,\quad \delta_4=\omega_4-\omega_1\ ,\end{aligned}\tag{A1}$$

and rewrite Eqs. (3.4) as

$$\begin{aligned}\dot{\xi}_1&=\delta_1+\cos(\xi_1+\xi_2)+\cos(\xi_1+\xi_2+\xi_3)\\&\quad-\cos(\xi_2)-\cos(\xi_2+\xi_3)\ ,\\\dot{\xi}_2&=\delta_2+\cos(\xi_2+\xi_3)+\cos(\xi_2+\xi_3+\xi_4)\\&\quad-\cos(\xi_3)-\cos(\xi_3+\xi_4)\ ,\\\dot{\xi}_3&=\delta_3+\cos(\xi_3+\xi_4)+\cos(\xi_3+\xi_4+\xi_1)\\&\quad-\cos(\xi_4)-\cos(\xi_4+\xi_1)\ ,\\\dot{\xi}_4&=\delta_4+\cos(\xi_4+\xi_1)+\cos(\xi_4+\xi_1+\xi_2)\\&\quad-\cos(\xi_1)-\cos(\xi_1+\xi_2)\ .\end{aligned}\tag{A2}$$

Taking into account that

$$\xi_1+\xi_2+\xi_3+\xi_4=0\ ,$$

one can obtain

$$\begin{aligned}\dot{\xi}_1&=\delta_1+\cos(\xi_1+\xi_2)+\cos(\xi_1+\xi_2+\xi_3)\\&\quad-\cos(\xi_2)-\cos(\xi_2+\xi_3)\ ,\\\dot{\xi}_2&=\delta_2+\cos(\xi_2+\xi_3)+\cos(\xi_1)\\&\quad-\cos(\xi_3)-\cos(\xi_1+\xi_2)\ ,\\\dot{\xi}_3&=\delta_3+\cos(\xi_2)+\cos(\xi_1+\xi_2)\\&\quad-\cos(\xi_1+\xi_2+\xi_3)-\cos(\xi_2+\xi_3)\ .\end{aligned}\tag{A3}$$

Equations (A3) can be viewed as equations for streamlines in stationary incompressible three-dimensional (3D) flow:

$$\dot{\boldsymbol{\xi}}=\mathbf{V}\ .\tag{A4}$$

Flow (A4) is solenoidal, which means that

$$\mathbf{V}=\nabla\times\mathbf{A},\quad \mathrm{div}\mathbf{V}=0\ .$$

Equations (A4) can be rewritten in more convenient form

$$\begin{aligned}\dot{\xi}_1&=\partial A_3/\partial\xi_2\ ,\\\dot{\xi}_2&=\partial A_1/\partial\xi_3-\partial A_3/\partial\xi_1\ ,\\\dot{\xi}_3&=-\partial A_1/\partial\xi_2\ ,\end{aligned}\tag{A5}$$

where A_i's are the components of the vector potential

$$\begin{aligned}A_1&=-\sin(\xi_2)-\sin(\xi_3)-\sin(\xi_1+\xi_2)+\sin(\xi_2+\xi_3)\\&\quad+\sin(\xi_1+\xi_2+\xi_3)+\delta_2\xi_3/2-\delta_3\xi_2\ ,\\A_2&=0\ ,\\A_3&=-\sin(\xi_1)-\sin(\xi_2)+\sin(\xi_1+\xi_2)-\sin(\xi_2+\xi_3)\\&\quad+\sin(\xi_1+\xi_2+\xi_3)-\delta_2\xi_1/2+\delta_1\xi_2\ ,\end{aligned}\tag{A6}$$

Equations (A5) are Hamiltonian equations in noncanonical variables, and can be deduced from the variation of the functional (action):

$$\delta S=\delta\int\mathcal{L}dt=0\ ,\tag{A7}$$

where the Lagrangian

$$\mathcal{L}=\mathbf{A}\cdot\dot{\boldsymbol{\xi}}\ .\tag{A8}$$

The explicit form of the functional on the right-hand side of (A7) is

$$S=\int(A_1d\xi_1+A_3d\xi_3)\ ,\tag{A9}$$

which leads to correspondence between systems (A5) and (A6) and a nonstationary Hamiltonian system with one degree of freedom, written in canonical variables (p,q):

$$\xi_1=q,\quad A_1'=p,\quad \xi_3=t,\quad A_3'=-H\ ,\tag{A10}$$

where

$$\begin{aligned}p&=-\sin(t)+4\sin(t/2)\cos(q/2)\\&\quad\times\cos(q/2+t/2+\xi_2)+\delta_2t/2-\delta_3\xi_2\ ,\\H&=\sin(q)-4\sin(q/2)\cos(t/2)\\&\quad\times\cos(q/2+t/2+\xi_2)+\delta_2q/2-\delta_1\xi_2\ .\end{aligned}\tag{A11}$$

The Hamiltonian H in standard notations has the following form:

$$H(p,q,t)=H_0(p,q,t)+\delta_2[q+t\tan(q/2)/\tan(t/2)]/2-[\delta_1+\delta_3\tan(q/2)/\tan(t/2)]\xi_2(p,q,t)\ ,\tag{A12}$$

where the unperturbed part of the Hamiltonian

$$H_0(p,x,t)=-p\tan(q/2)/\tan(t/2)+\sin(q)-\sin(t)\tan(q/2)/\tan(t/2) \tag{A13}$$

is a linear function of momentum p, and function $\xi_2(p,q,t)$ is defined as the solution of the Bessel equation:

$$\delta_3\xi_2+p+\sin(t)-\delta_2 t/2=4\sin(t/2)\cos(q/2)\cos(q/2+t/2+\xi_2)\ . \tag{A14}$$

The unperturbed system with $\delta=0$ is degenerate because $\partial^2 H_0/\partial p^2\equiv 0$. This degeneracy can be removed by simple canonical transformation with the generating function:

$$W(P,q,t)=P\sin(q/2)\sin(t/2)+\sin(q)\sin(t)\ . \tag{A15}$$

The connection between new (P,Q) and old (p,q) canonical pairs is given by the following equations:

$$\begin{aligned} Q&=\partial W/\partial P=\sin(q/2)\sin(t/2)\ , \\ p&=\partial W/\partial q=(P/2)\cos(q/2)\sin(t/2)+\cos(q)\sin(t)\ . \end{aligned} \tag{A16}$$

One can call these new variables (P,Q) "slow variables," because their time rate is proportional to small parameters δ_i. Hamiltonian (A12) in slow variables is also proportional to δ_i,

$$H'(P,Q,t)=H+\partial W/\partial t=\delta_2[q+t\tan(q/2)/\tan(t/2)]/2-[\delta_1+\delta_3\tan(q/2)/\tan(t/2)]\xi_2(p,q,t) \tag{A17}$$

where q, p, and ξ_2 should be expressed as functions of Q, P, and t.

[1] V. I. Arnold, *Mathematical Methods in Classical Mechanics* (Springer, Berlin, 1978).

[2] A. A. Chernikov, R. Z. Sagdeev, and G. M. Zaslavsky, Today, **41**(11), 27 (1988); G. M. Zaslavsky, R. Z. Sagdeev, D. A. Usikov, and A. A. Chernikov, *Weak Chaos and Quasiregular Patterns* (Cambridge University Press, Cambridge, 1991).

[3] A. A. Chernikov and G. Schmidt, Phys. Lett. A **169**, 51 (1992).

[4] K. Y. Tsang, R. E. Mirollo, S. H. Strogatz, and K. Wiesenfeld, Physica D **48**, 102 (1991).

[5] J. W. Swift, S. H. Strogatz, and K. Wiesenfeld, Physica D **55**, 239 (1992).

[6] S. Watanabe and S. H. Strogatz, Phys. Rev. Lett. **70**, 2391 (1993); and (unpublished).

[7] M. B. Sevryuk, *Reversible Systems,* Lecture Notes in Mathematics Vol. 1211 (Springer, Berlin, 1986).

[8] A. I. Neishtadt, Prikl. Mat. Mech. **51**, 750 (1975) [J. Appl. Math. Mech. **39**, 594 (1975)].

[9] S. M. Carioli, A. A. Chernikov, and A. I. Neishtadt, Phys. Scr. **40**, 707 (1989); A. A. Chernikov, G. Schmidt, and A. I. Neishtadt, Phys. Rev. Lett. **68**, 1507 (1992).

[10] A. I. Neishtadt, Chaos **1**, 42 (1991).

[11] I. M. Lifshitz, A. A. Slutskin, and V. M. Nabutovskii, Zh. Eksp. Teor. Fiz. **41**, 939 (1961) [Sov. Phys. JETP **14**, 669 (1962)].

[12] A. I. Neishtadt, D. K. Chaikovsky, and A. A. Chernikov, Zh. Eksp. Teor. Fiz. **99**, 763 (1991) [Sov. Phys. JETP **72**, 423 (1991)].